2201
RB → Jenny

Electro-optically controlled beam deflection for grazing incidence geometry on a domain-engineered interface in $LiNbO_3$

Robert W Eason*, Alexander J Boyland, Sakellaris Mailis, Peter G R Smith.

Optoelectronics Research Centre

University of Southampton

Southampton

SO17 1BJ

U.K.

* corresponding author:

Tel 023 80592098: Fax 023 80593142: e-mail rwe@orc.soton.ac.uk

Submitted to opt. comm

April '01

Key-words: Lithium Niobate, electro-optic effect, domain-engineering, beam scanning, beam deflection.

Abstract.

We report an analysis on the electro-optically induced beam deflection experienced by light traversing an interface between two anti-parallel domains in a sample of $LiNbO_3$. In contrast to other work on prism deflection schemes, we present a grazing incidence geometry for light at incidence angles between 87° and 89.5° that has been investigated to maximise the deflection angles achievable. Further improvements can be obtained for both range of angular deflection and transmission uniformity, by faceting the exit face of the device at an optimum angle. We present a theoretical analysis for this configuration and compare with data obtained for a wavelength of 1.52μm. A practical geometry would permit a deflection of ~140mrad for an applied voltage of 1kV.

1. Introduction.

Solid-state devices developed for beam scanning and deflection have been widely reported in the recent past. Requirements of speed, compactness and integration have favoured the use of domain-engineered samples of ferroelectrics such as $LiNbO_3$ and $LiTaO_3$ that permit electro-optic control of local refractive index, thereby enabling small changes in propagation direction via refraction at an interface. Prism type geometries are perhaps the most reported to date, in which light is incident on a series of triangular domain-inverted regions, the deflection angles achievable being a function of both geometry and number of prisms [1-2]. Further levels of integration have also been reported, in which scanning has been integrated with focussing elements [3], second harmonic generation [4], and for use as a laser Q-switch [5].

Although recent work has addressed the problem of optimising the design of such electro-optic prism scanners, and also discussed the alternative gradient index deflectors, where the light ray is bent as it propagates through a region of non-uniform refractive index [6], there remains a fundamental problem with this approach. The linear electro-optic effect in $LiNbO_3$ or $LiTaO_3$ is comparatively weak, and at moderate field strengths of ~1kV mm^{-1}, the deflection angles achievable are small. As an illustration of this limitation, we show below calculations of deflection angle, δ, achieved for a single e-o prism deflector under four different electric field addressing geometries..

The equation relating the induced refractive index change, Δn, under electro-optic addressing, as a function of electric field strength E_z is given by the usual expression below:

$$\Delta n = - \tfrac{1}{2} r_{33} n_e^3 E_z \qquad (1)$$

where r_{33} is the largest electro-optic coefficient accessed by extraordinary polarised light, n_e is the wavelength dependent value of extraordinary refractive index, and E_z is the electric field strength applied across the sample in the z-direction.

For simplicity, and as a means of comparison between existing electro-optic prism designs and our near total internal reflection geometry, we standardise on a common set of values for refractive index, electro-optic coefficient, and value of applied electric field strength. These are: $n_e = 2.23$, $r_{33} = 30.8 \times 10^{-12}$ mV^{-1}, and $E_z = 1kV\ mm^{-1}$ (10^6 Vm^{-1}), which relate to congruent single crystal $LiNbO_3$ for light in the mid-visible region of the spectrum at ~550nm. Shown in figure 1 is the familiar geometry for beam deflection via a prism of apex angle α. For electro-optic addressing there are four possible conditions for producing beam deflection when an electric field is applied to either the prism and/or the background host material. Values of deflection angle may be increased by a factor of two by simultaneously increasing one refractive index (e.g. n_2), while reducing the other (n_1) by the same amount, as is the case for a uniform field applied to a domain inverted sample. Additionally, as has been demonstrated in [3] for example, prisms can be cascaded so that the achievable deflection angles are increased as a linear function of the number of prisms. Finally, as the beam emerges into air from a medium of refractive index ~2.2, there is a final

magnification of the deflection achieved by this same factor, in the small deflection limit.

Table 1 shows the calculated values of beam deflection angle for these four different geometries, for a common angle of incidence of 30°, at an applied electric field of 1kV mm^{-1}. Of note here are the small values obtained for δ, which have been calculated for a single prism of apex angle 60°, for the four possible combinations of n_2/n_1, which we abbreviate to n_{21}. Even for the most favourable case where $n_1 = n-\Delta n$, and $n_2 = n+\Delta n$, the deflection angle achieved is only 0.01°. In [3], where seven prisms are used in series, and the applied field was ~4.4kV mm^{-1}, this produces a total deflection angle of ~0.3°, which is magnified to ~0.66° when the beam is refracted into the air. In [3] where α was of order 66°, the reported beam deflection was 0.72° (12.65 mrad).

Figure 2 shows exact calculations of deflection angle δ for the four possible electro-optic geometries, using the following equation for beam deflection via a prism of apex angle α [7]:

$$\delta = \theta_i - \alpha + \sin^{-1} \{ \sin \alpha [(n_{21})^2 - \sin^2 \theta_i]^{1/2} - \sin \theta_i \cos \alpha \} \qquad (2)$$

where θ_i is the angle of incidence. As expected the plots are symmetrical about the zero deflection line, but what is immediately apparent is that the ~30° angles typically used for θ_i in prism scanners represents the precise angle for which minimum deviation is produced. This choice of angle is necessary however when cascaded prisms are used as in [3], and in-line prism fabrication is the preferred route.

It is therefore apparent that the single prism deflection result of ~0.01° for a normalised value of applied electric field of 1kV mm^{-1} may be increased if alternative geometries are adopted. This paper discusses the use of a near total internal reflection (TIR) geometry, which we have already successfully used to demonstrate a switch with a measured contrast ratio exceeding 100:1 [8]. In this implementation however, it is the deflection of the transmitted beam we are considering, rather than the switching into TIR.

2. TIR beam deflection geometry.

Figure 3 shows a schematic of the electro-optic TIR geometry for a domain engineered $LiNbO_3$ switch/scanner. The sample was a 300 μm thick z-cut congruent $LiNbO_3$ wafer supplied by Yamaju (Japan), with dimensions in the x and y directions of 13.5 mm x 15mm. The –z face was photolithographically patterned and electric field poled to produce a structure consisting of two anti-parallel domains. Under polarised light microscopic examination, the interface layer was seen to be quite flat and smooth, but some fine detail, including local variation from absolute straightness was observed in all the engineered samples produced. After poling, annealing was performed at 200°C for several hours, to attempt to remove any residual strain at the interface. Experiments performed for TIR switching however revealed that even after annealing a small residual refractive index existed across this interface which was of order 10^{-5} [8].

Experiments were performed using the two laser wavelengths of 0.543μm and 1.523μm from separate polarised He-Ne laser sources, both of output power ~0.6mW.

Focussing into the $LiNbO_3$ sample was achieved by a lens of focal length 160mm, which produced a spot size of order 40 μm for the 0.543 μm light. Electrodes were fabricated on both + and –z faces, of dimensions ~12mm x 2mm, across the domain interface region. The input and exit faces were parallel polished, and the device was mounted on an insulating support.

Before characterising the scanner performance, simulations were run based on the change of the refracted ray direction at the electro-optically addressed interface. Unlike the case for electro-optic prism scanning, the grazing incidence geometry is uniquely sensitive to small changes of local index. Applying Snell's law to the interface yields:

$$(n+\Delta n) \sin \theta_i = (n- \Delta n) \sin \theta_t \qquad (3)$$

where Δn is as defined in (1).

Figure 4 shows values of θ_t calculated via (3), as a function of voltage applied across the interface, for values of θ_i ranging from 87° to 89.5° in 0.5° steps. It is immediately apparent that even for modest voltages of order a few hundred volts, substantial deflections of ~1° can be obtained. For the θ_i =87° case, a line has been drawn through the points to illustrate that the relationship at such angles is effectively linear for this voltage range. For the case of θ_i =88.5°, a value we have investigated experimentally and is relatively easy to implement in a sample of interface length ~10mm, a voltage of 300V (corresponding to the normalised value of 1kV mm^{-1} across the 300μm thick sample) produces an angular deflection of 0.39°. When compared to the value of angular deflection for the single prism deflector evaluated earlier, we see that this near TIR geometry is ~40 times higher in sensitivity.

Two further points to note in figure 4 are that we only present the deflection for one polarity of applied field. If the polarity of the applied field is reversed, there is a corresponding increase in deflection angle achievable, as well as the additional possibility of improved linearity. As the deflection increases, TIR occurs at the value of θ_t=90° as shown in the figure.

As the deflection angle increases, and TIR is approached, the transmitted intensity across the interface decreases. This is an important factor that must be addressed when considering the acceptable operating parameters of such a device. Figure 5 shows the transmitted intensity calculated for the same range of applied field as shown in figure 4. While it is clear that for values of $\theta_i > 89°$, the transmission falls rapidly as a function of applied field, for a value of $\theta_i < 88°$ the slope is small, and some degree of linearity again exists between transmission and applied field.

We can compare these results with those obtained experimentally using 's' polarised light from an I.R. He-Ne laser operating at 1.523μm. Figures 6 and 7 show the results for transmitted angle, θ_t, and transmitted power versus the applied field over the same range as calculated earlier. It is seen that the overall shape is very similar to the theoretical plots of figures 4 and 5, allowing for both the uncertainty of the *absolute* value of θ_i which is difficult to measure precisely at such steep grazing incidence angles and carries an estimated uncertainty of order 0.1-0.2°, and also the fact that the interface is not straight at the better than 0.1° level. A final difference between the theoretical plots and the experimental data is that the beam is focussed to a waist at the middle point of the device, and hence some divergence, will occur in the wings of the Gaussian beam, which intersect the interface at a point other than the middle of

the device. We are currently modelling this behaviour that will modify the shape of the plots obtained, rather than introduce the small noise we see in the measurement of both angle and transmitted power. We will shortly be fabricating such domain interfaces in stoichiometric rather than congruent $LiNbO_3$ and we expect that the interface quality will be better.

3. Improvements to the device linearity.

There is a final improvement that can be made to the performance of the device in terms of the linearity and range of the deflection angle obtained, and which simultaneously flattens the transmitted intensity characteristics. Figure 8 shows a simple modification to the output end of the sample, in which a facet is polished at an angle of β or γ respectively. The facet acts to magnify the angular deflection via the normal Snell law of refraction into a less dense medium, and if the angle is chosen appropriately, there is also a compensating behaviour for the previous transmission drop and the nonlinearity of angular deflection.

Figure 9 illustrates this behaviour for a value of $\theta_i = 87.75^\circ$ for a facet angled as shown in figure 8(a). In this geometry however, although the external angle of deflection is substantially increased when compared to that through an end face polished normally to the ray direction, the linearity is poor. Nevertheless, for $\beta = 62.5^\circ$ a deflection of $\sim 8^\circ$ is achievable for the voltage range between 0- 1000V. For the normalised value of 1kV mm^{-1} an angular deflection of 1.6° is achieved compared to a value of 0.5° without the exit facet.

When the facet is angled the opposite way, as shown in figure 8(b), then the opportunity exists to simultaneously have a large deflection range, and good linearity of deflection and transmission as a function of voltage applied. Although the linearity of deflection is not an intrinsic necessity, and can be calibrated out, it is a desirable attribute if implementation is easy. Figures 10 and 11 show similar calculations for this oppositely angled facet. As θ_t increases, the value of θ_γ decreases, thereby reducing the Fresnel reflectivity from this angled facet and acting to compensate for the decreasing value of transmission across the interface. Figures 10 and 11 show plots for facet angles spanning the range 66° to 70°. Figure 12 presents a final comparison between a facet angled at 69° and a facet polished at effectively normal incidence. Although greater Fresnel reflectivity invariably occurs for this 's' polarised state at these angles, it is immediately apparent that the transmission reduction has been at least partially compensated. For this geometry ($\theta_i = 87.75°$), this compensation is at the expense of an overall reduction of ~27% of the transmitted intensity.

4. Conclusions.

In conclusion we have presented a novel electro-optic beam deflector geometry, which permits a wide angular scan range, with simultaneous capability for good linearity of both deflection angle and transmission uniformity as a function of applied field. When compared to existing schemes for electro-optic scanning based on prisms, it is seen that this new geometry has a sensitivity that is between one and two orders of magnitude larger. We have shown that this geometry can function well as a beam deflector at the useful telecoms wavelength of 1.52μm.

5. Acknowledgements.

The authors are grateful to the Engineering and Physical Sciences Research Council (EPSRC) for funding for AJB and for research funding via grant no. GR/N00302.

6. References.

1. J.Li, H.C.Cheng, M.J.Kawas, D.N.Lambeth, T.E.Schlesinger, D.D.Stancil, 'Electro-optic wafer beam deflector in $LiTaO_3$', IEEE Photonics Technol. Lett., **8**, pp1486-1488, (1996)
2. Q.Chen, Y.Chiu, D.N.Lambeth, T.E.Schlesinger, D.D.Stancil, 'Guided-wave electro-optic beam deflector using domain reversal in $LiTaO_3$', J.Lightwave Technol, **12**, pp1401-1404, (1994)
3. K.T.Gahagan, V.Gopalan, J.M.Robinson, Q.X.Jia, T.E.Mitchell, M.J.Kawas, T.E.Schlesinger, D.D.Stancil, 'Integrated electro-optic lens/scanner in a $LiTaO_3$ single crystal', Appl. Opt., **38**, pp1186-1190, (1999)
4. Y.Chiu, V.Gopalan, M.J.Kawas, T.E.Schlesinger, D.D.Stancil, 'Integrated optical device with second-harmonic generator, electro-optic lens, and integrated scanner in $LiTaO_3$', J.Lightwave Technol., **17** pp462-465, (1999)
5. K.S.Abedin, T.Tsuritani, M.Sato, H.Ito, K.Shimamura, T.Fukuda, 'Integrated electrooptic Q switching in a domain-inverted Nd:$LiTaO_3$ laser', Opt.Letts., **20**, pp1985-1987, (1995)
6. Y.Chiu, J.Zou, D.D.Stancil, T.E.Schlesinger, 'Shape-optimized electrooptic beam scanners: analysis, design, and simulation', J.Lightwave Technol. **17**, pp108-114, (1999)
7. E.Hecht 'Optics' Addison-Wesley, (1998)
8. A.J.Boyland, G.W.Ross, S.Mailis, P.G.R.Smith, R.W.Eason, 'Total internal reflection switching in electro-optically addressable domain-engineered $LiNbO_3$, Submitted to Elec, Letts. (2000).

7. Figure Captions.

Figure 1. Schematic of refraction through a prism of refractive index n_2 in a host medium of index n_1. Overall angular deflection is δ.

Figure 2. Angle of deflection δ as a function of angle of incidence θ_i for n_{21} values as shown in table 1.

Figure 3. (a). Schematic of domain engineered sample used for beam scanning. Input light is 's' polarised.

Figure 3 (b) Plan view of scanner showing angles referred to in the text.

Figure 4. Transmitted angles θ_t as a function of voltage applied for a range of values of θ_i from 87.0° to 89.5°. For $\theta_i = 87.0°$, the line is a guide for the eye only.

Figure 5. Intensity transmission across the interface as a function of voltage applied, for a range of values of θ_i from 87.0° to 89.5°.

Figure 6. Experimental results obtained for transmitted angles θ_t as a function of voltage applied for two representative values of θ_i.

Figure 7. Experimental results for transmitted power (arb units) as a function of voltage applied for two representative values of θ_i.

Figure 8. Schematic of scanners with polished exit facets. The beam exits the rear face with angles of incidence θ_β (a) and θ_γ (b) respectively.

Figure 9. External angle of deflection θ_o as a function of voltage applied, for the arrangement of figure 8(a), for facet angles β between 62.5° and 64.0°. The value of θ_i here is 87.75°

Figure 10. External angle of deflection θ_o as a function of voltage applied, for the arrangement of figure 8(b), for facet angles γ between 66.0° and 69.0°. The value of θ_i here is 87.75° (lines drawn as guides for the eye only)

Figure 11. External intensity transmission for the arrangement of figure 8(b)as a function of voltage applied, for facet angles γ between 67.0° and 70.0°. The value of θ_i here is 87.75°

Figure 12. Comparison between transmission with and without rear faceting, as a function of voltage applied.

Table 1. Four combinations of indices n_1 and n_2 for electro-optic addressing of prism and/or host material, and resultant values of n_{21} and associated value of δ.

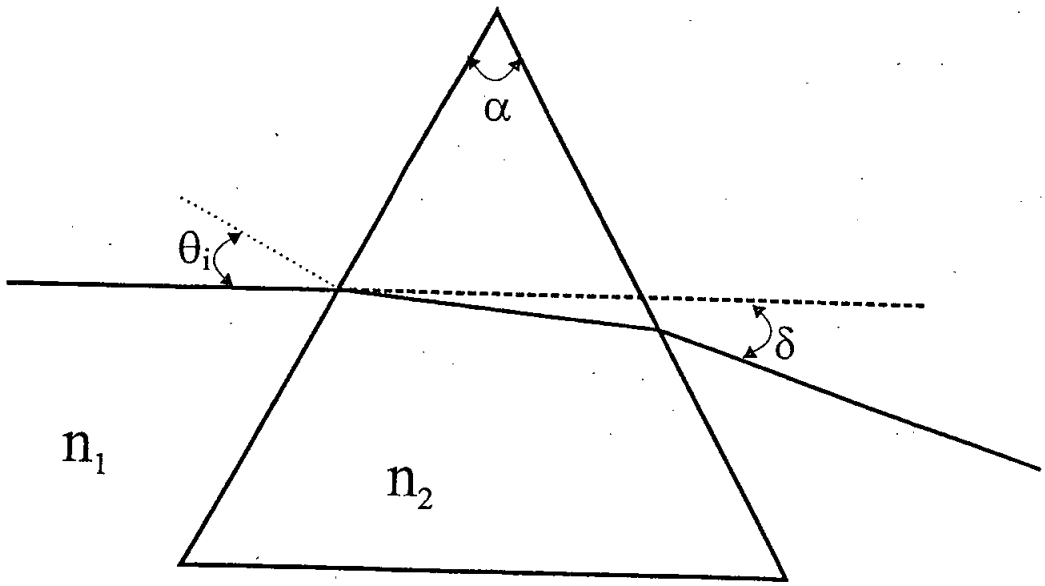

Fig 1

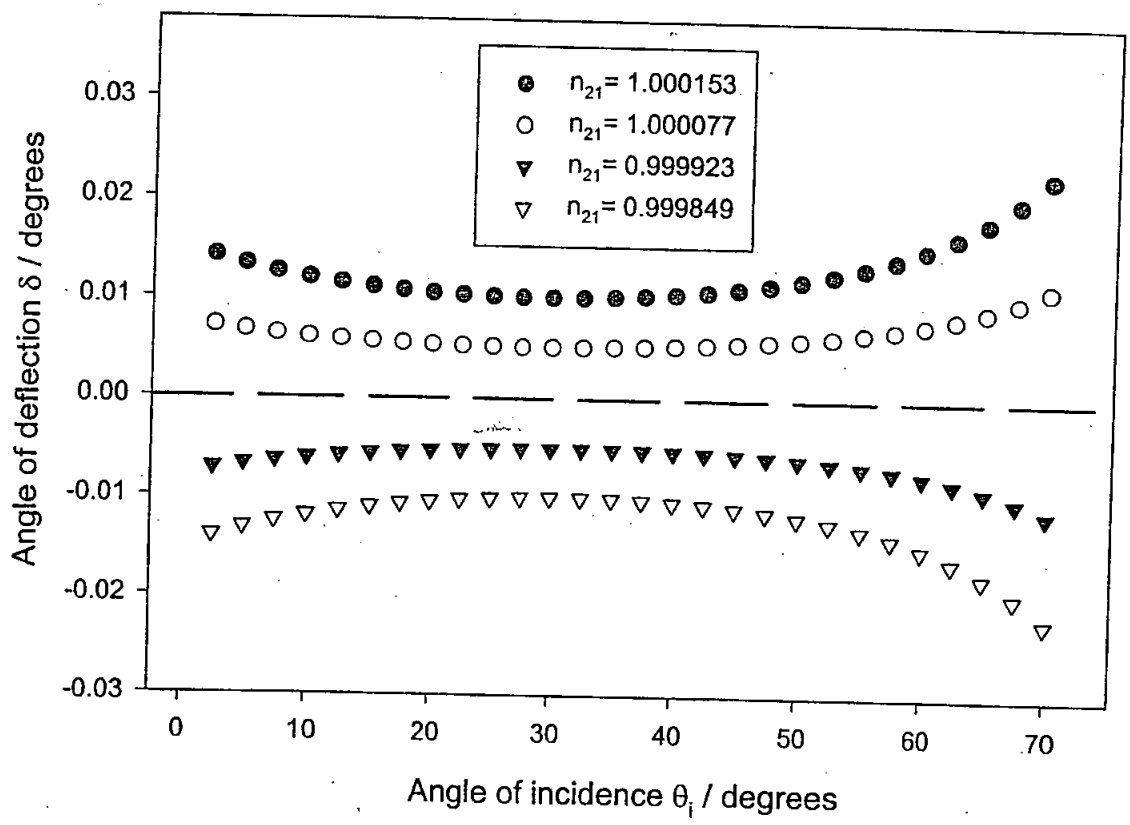
n_{21}= 1.000153
n_{21}= 1.000077
n_{21}= 0.999923
n_{21}= 0.999849
0.03
0.02
0.01
0.00
-0.01
-0.02
-0.03
0
10
20
30
40
50
60
70
Angle of deflection δ / degrees
Angle of incidence θ_i / degrees

Fig 2

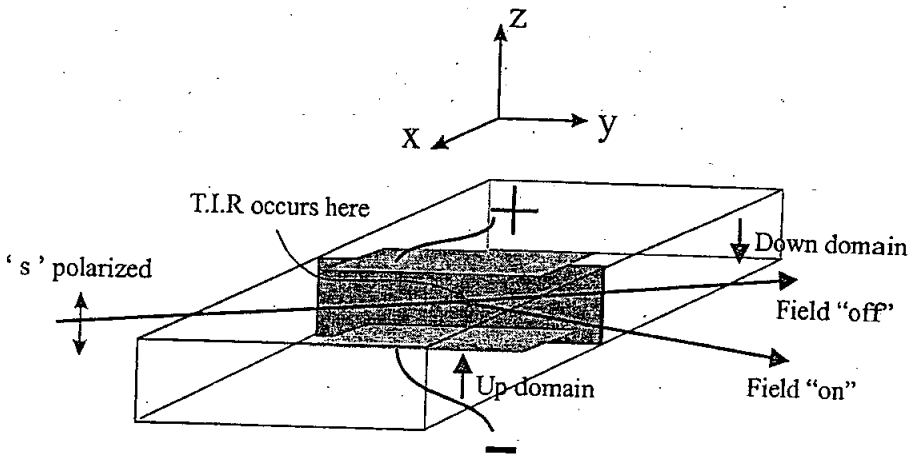
z
x
y
T.I.R occurs here
' s ' polarized
Down domain
Field "off"
Up domain
Field "on"
+
−

(a)

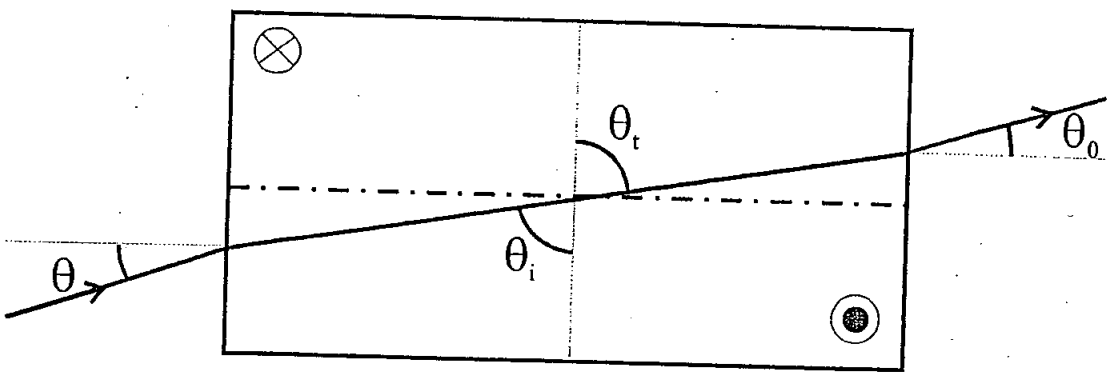
θ
θi
θt
θ0

(b)

Figure 3

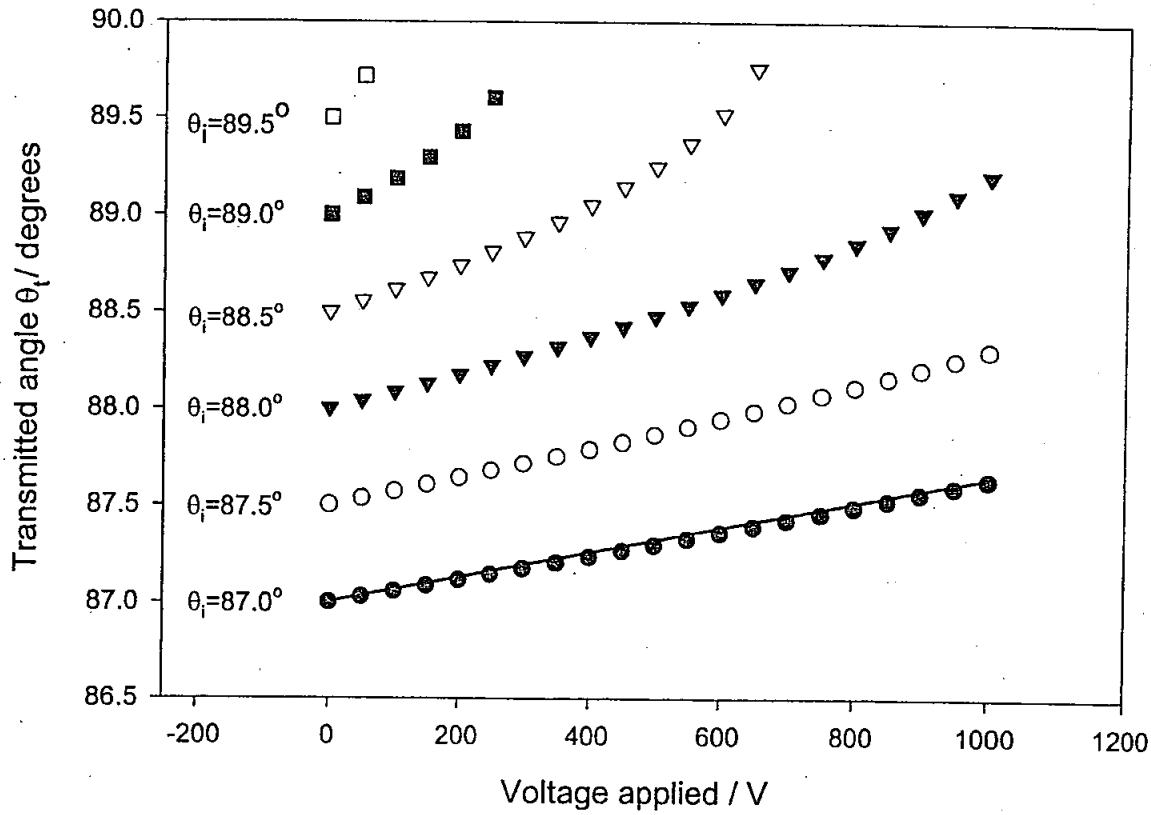
90.0
89.5
89.0
88.5
88.0
87.5
87.0
86.5
θi=89.5°
θi=89.0°
θi=88.5°
θi=88.0°
θi=87.5°
θi=87.0°
Transmitted angle θt / degrees
-200
0
200
400
600
800
1000
1200
Voltage applied / V

Fig 4

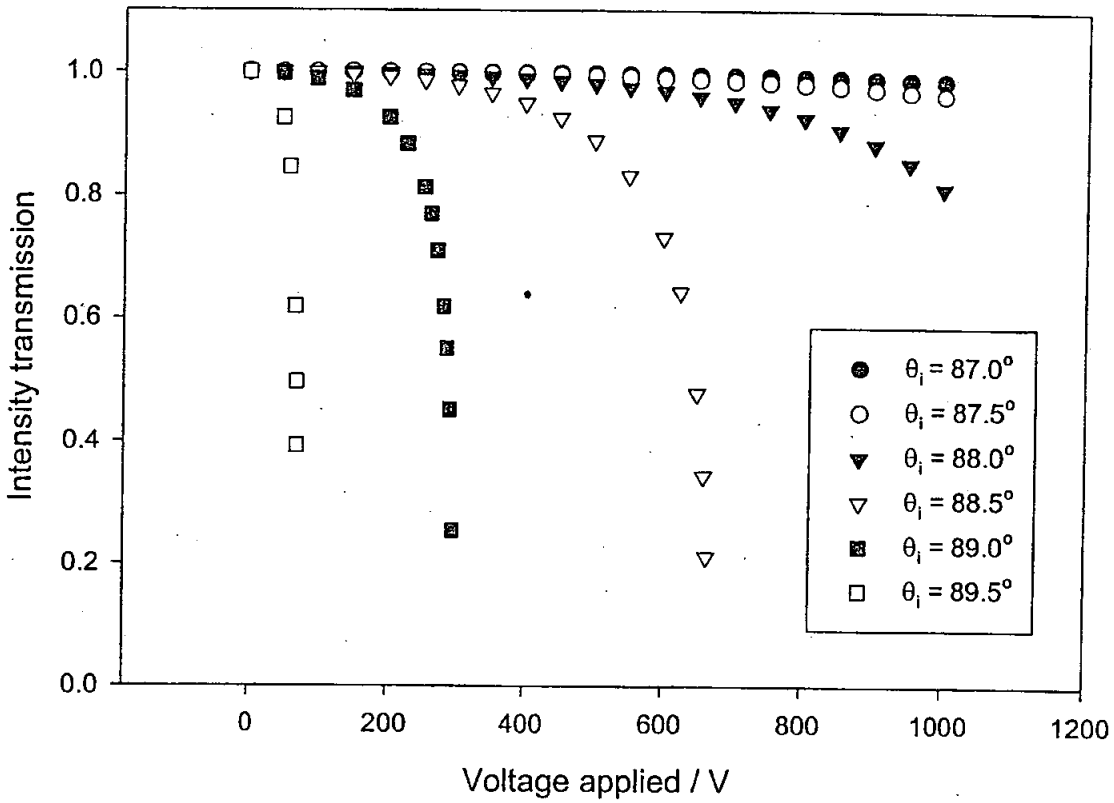
Intensity transmission
1.0
0.8
0.6
0.4
0.2
0.0
0
200
400
600
800
1000
1200
Voltage applied / V
θi = 87.0°
θi = 87.5°
θi = 88.0°
θi = 88.5°
θi = 89.0°
θi = 89.5°

Fig 5

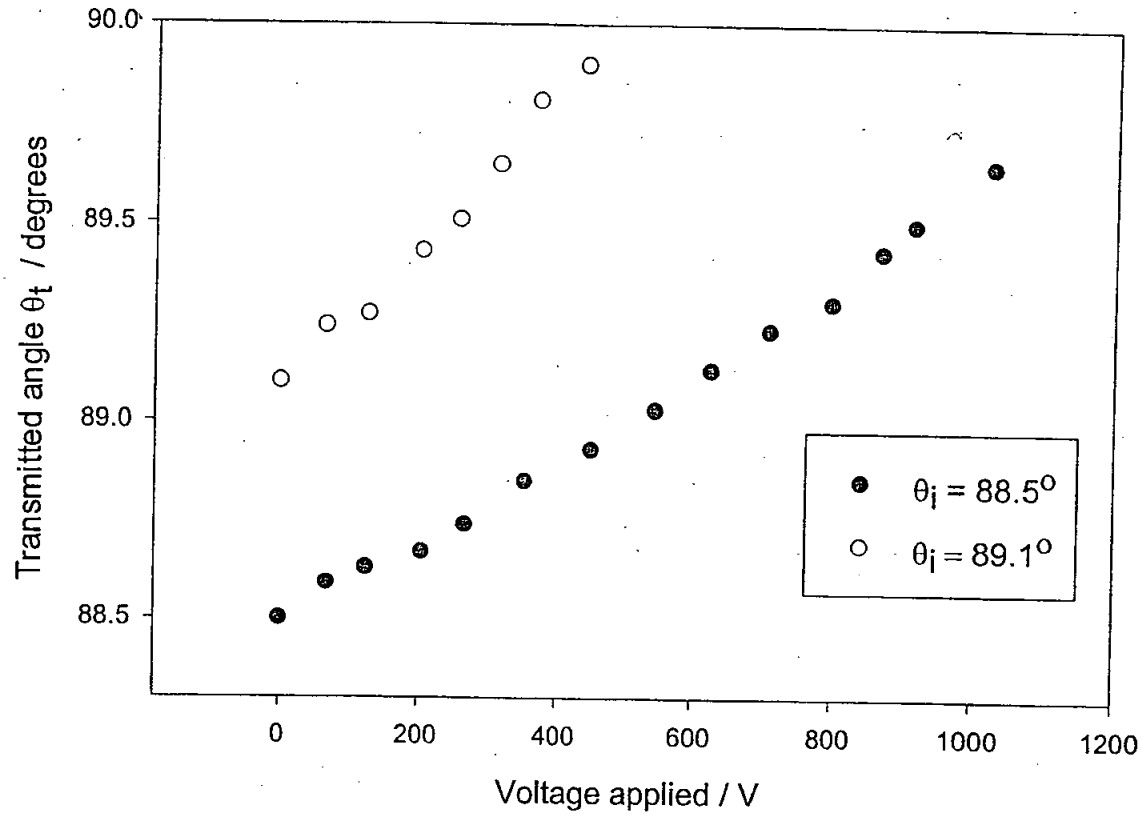
90.0
89.5
89.0
88.5
Transmitted angle θt / degrees
0
200
400
600
800
1000
1200
Voltage applied / V
θi = 88.5°
θi = 89.1°

Fig 6

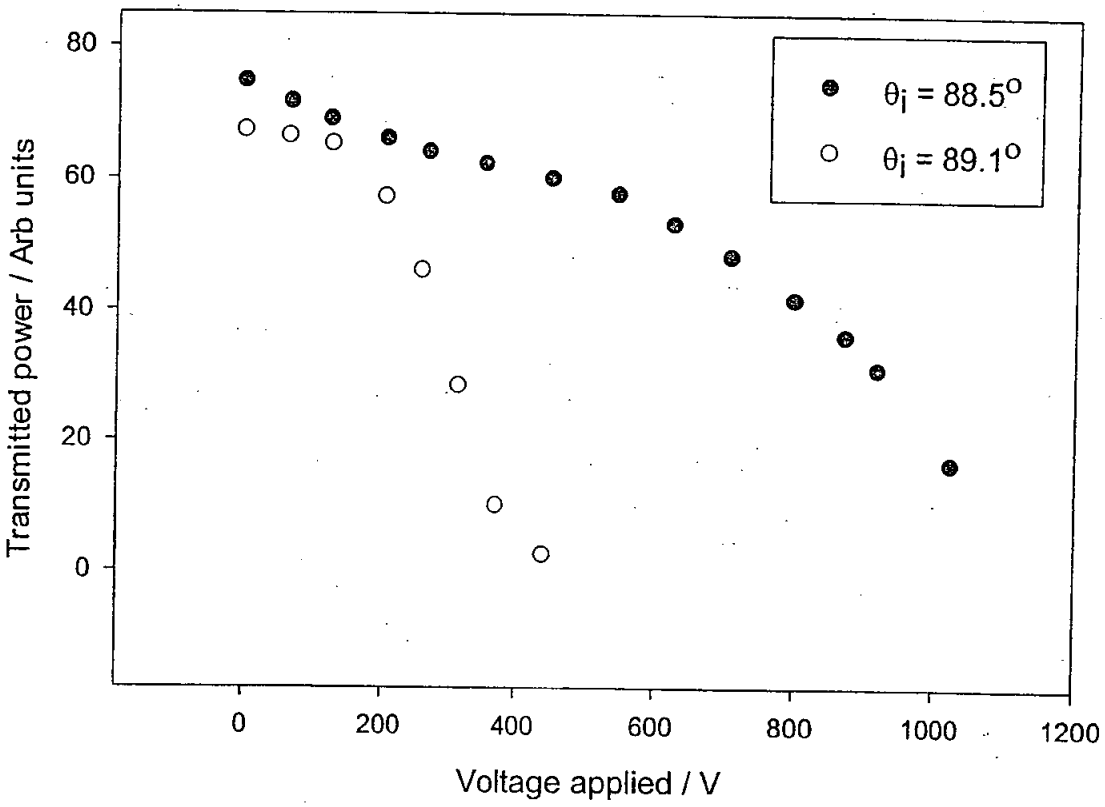
Transmitted power / Arb units
Voltage applied / V
θi = 88.5°
θi = 89.1°
0
20
40
60
80
0
200
400
600
800
1000
1200

Fig 7

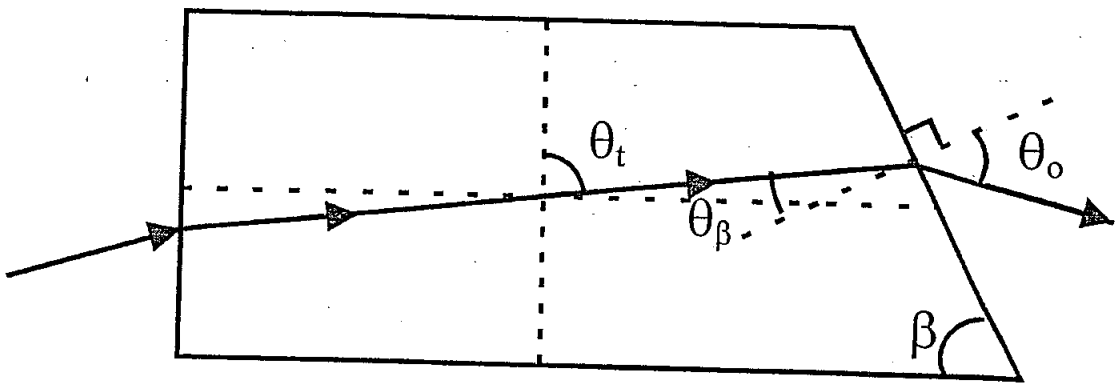

a)

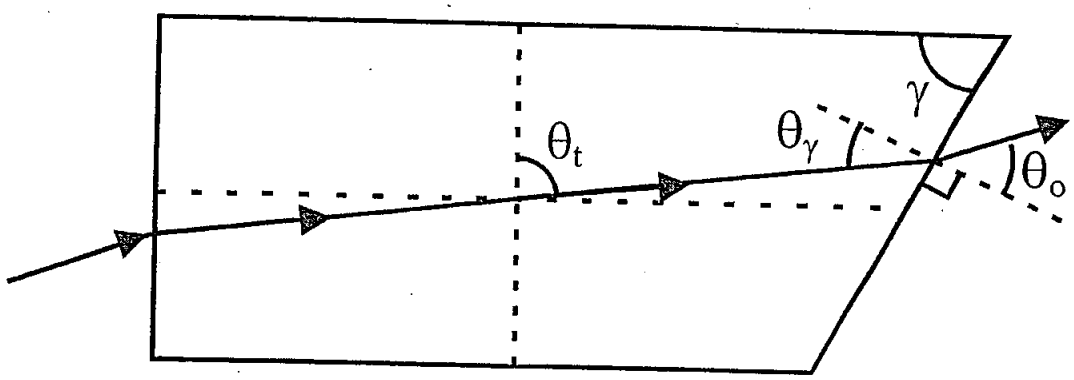

b)

Fig 8

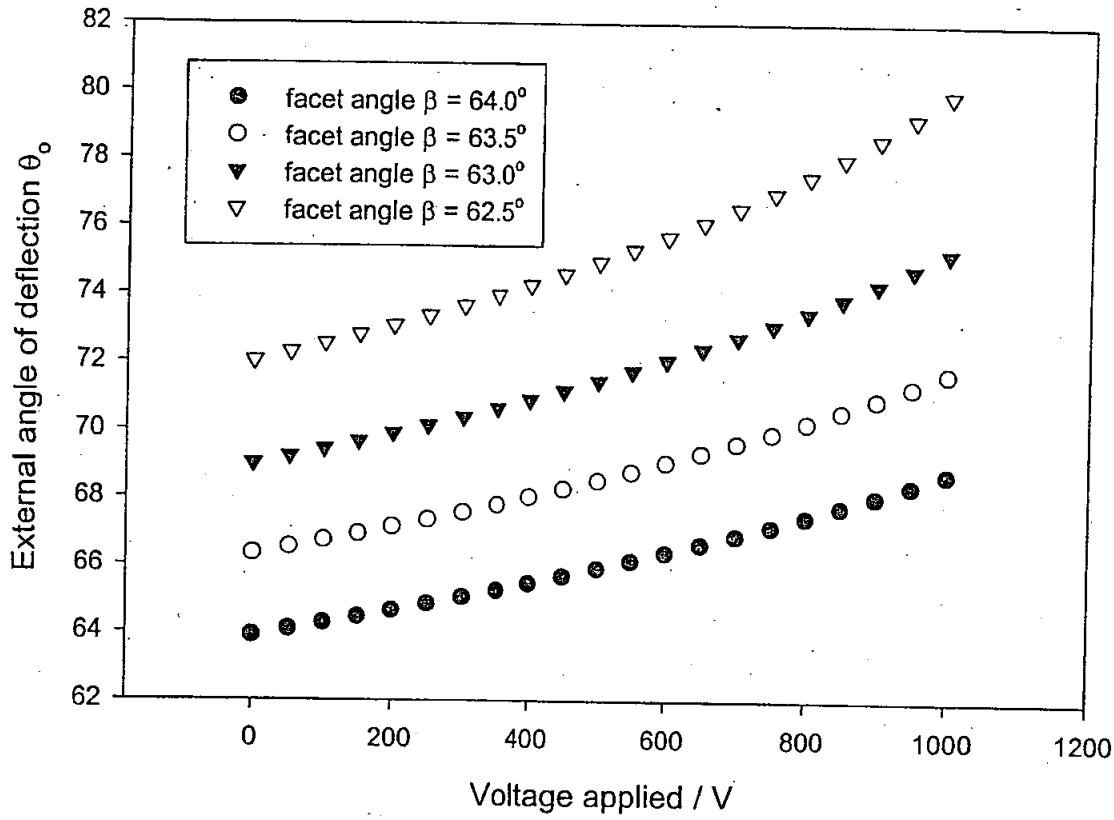
facet angle β = 64.0°
facet angle β = 63.5°
facet angle β = 63.0°
facet angle β = 62.5°
External angle of deflection θo
Voltage applied / V
82
80
78
76
74
72
70
68
66
64
62
0
200
400
600
800
1000
1200

Fig 9

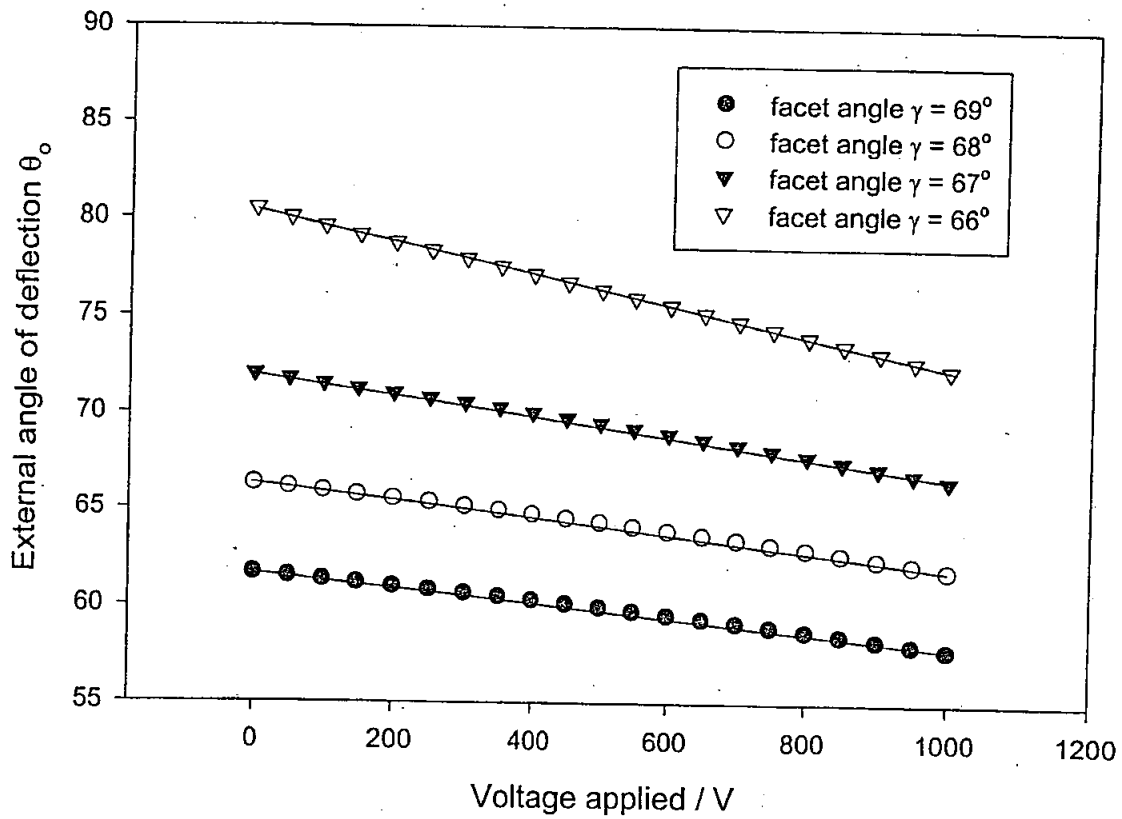
90
85
80
75
70
65
60
55
External angle of deflection θ_o
0
200
400
600
800
1000
1200
Voltage applied / V
facet angle γ = 69°
facet angle γ = 68°
facet angle γ = 67°
facet angle γ = 66°

Fig 10

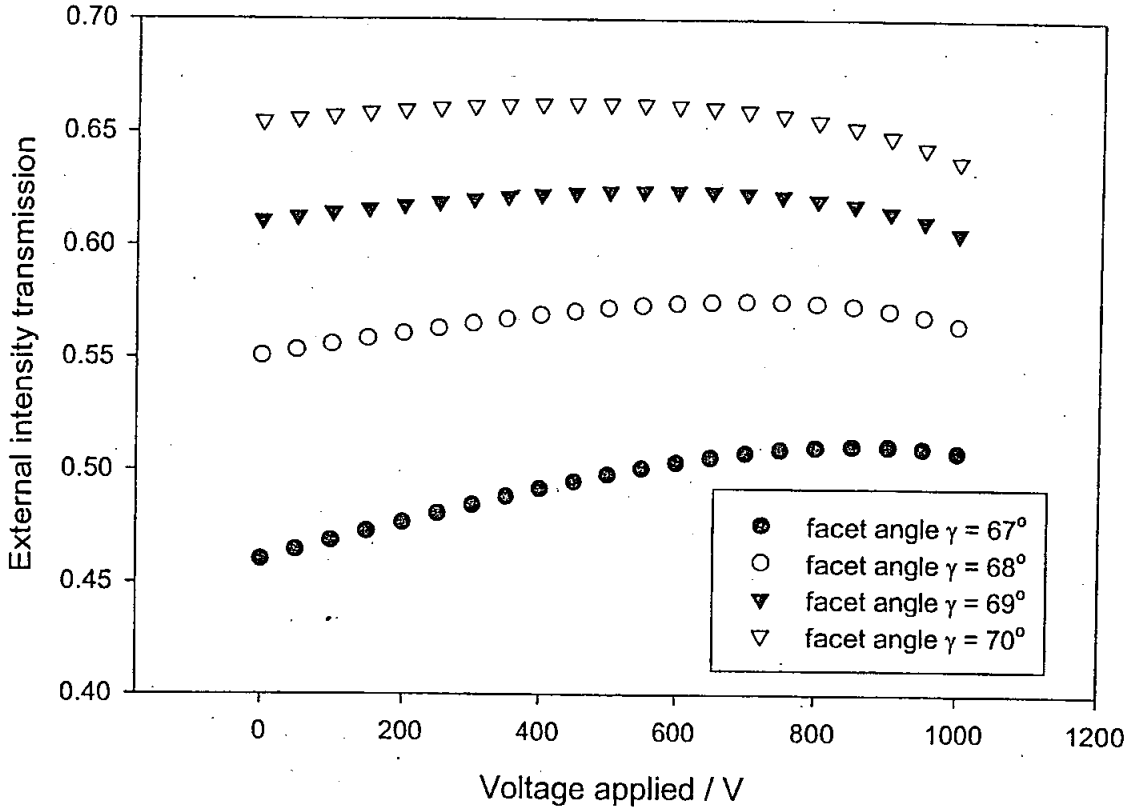
External intensity transmission
0.70
0.65
0.60
0.55
0.50
0.45
0.40
0
200
400
600
800
1000
1200
Voltage applied / V
facet angle γ = 67°
facet angle γ = 68°
facet angle γ = 69°
facet angle γ = 70°

Fig 11

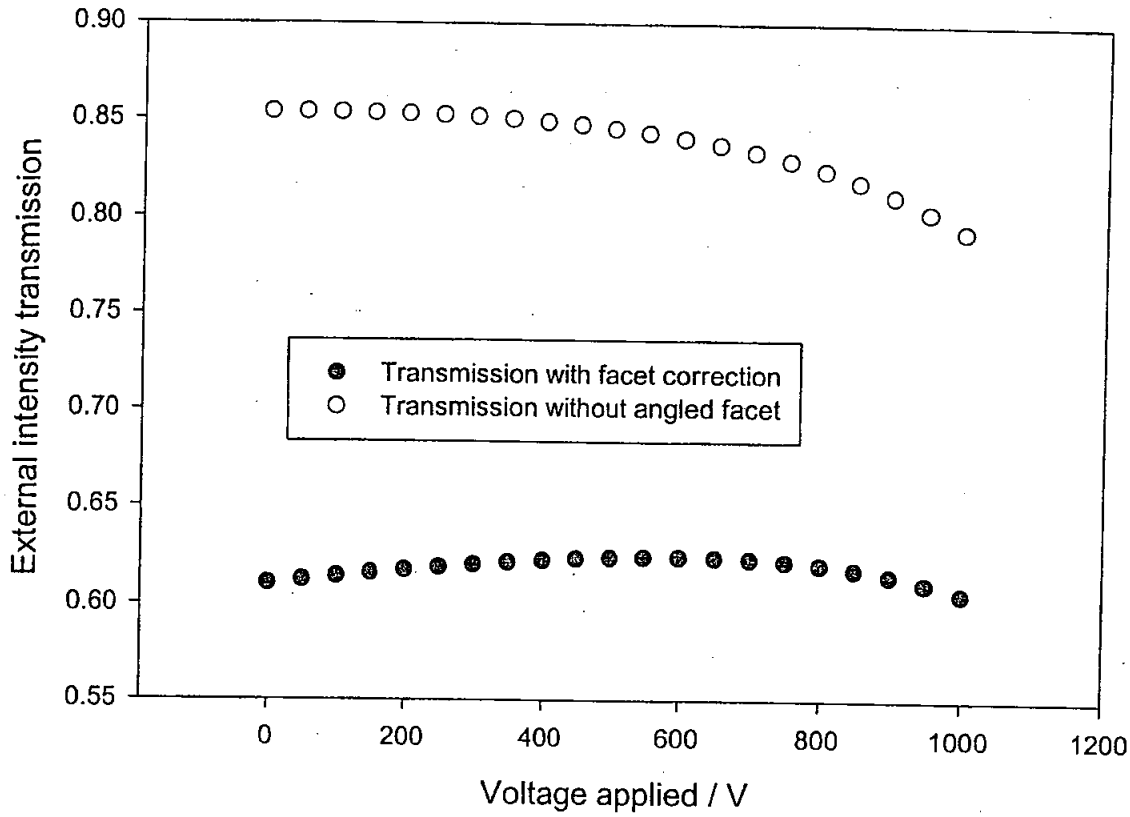
0.90
0.85
0.80
0.75
0.70
0.65
0.60
0.55
External intensity transmission
Transmission with facet correction
Transmission without angled facet
0
200
400
600
800
1000
1200
Voltage applied / V

Fig 12

n_1	n_2	$n_{21} = n_2/n_1$	δ / degrees
$n-\Delta n$	$n+\Delta n$	1.000153	0.010
n	$n+\Delta n$	1.000077	0.005
$n+\Delta n$	$n-\Delta n$	0.999849	-0.005
n	$n-\Delta n$	0.999923	-0.010

Table 1